3000 CA Rotterdam
the Netherlands
E-mail: a.vandersteen@erasmusmc.nl

http://dx.doi.org/10.1016/j.jcmg.2015.08.010

Please note: Drs. Wang, Regar, Beusekom, Lancee, Springeling, Krabbendam-Peters, van der Steen, and van Soest are from the Department of Cardiology, Erasmus University Medical Center, Rotterdam, the Netherlands; Drs. Pfeiffer, Wieser, and Huber are from Lehrstuhl für Biomolekuläre Optik, Fakultät für Physik, Ludwig-Maximilians-Universität Munchen, Germany; and Drs. Pfeiffer and Huber are from the Institut für Biomedizinische Optik, Universität zu Lübeck, Lübeck, Germany. This research was partly supported by the China Scholarship Council, the German Research Foundation (DFG-HU 1006/2, HU 1006/3, Cluster of Excellence: Munich Centre for Advanced Photonics), and the European Union (ERC, contract no. 259158). Mr. Wieser has a financial interest in Optores GmbH, which commercializes Fourier domain mode-locked technology for nonvascular applications. Prof. Huber has a financial interest in Optores GmbH; and holds a patent licensed to St. Jude Medical. All other authors have reported that they have no relationships relevant to the contents of this paper to disclose.

The authors acknowledge J. Meijer and B. Knapen from KINETRON B.V. for manufacturing the micro motor, and C. Niles and R. van Duin for their contributions in the animal experiment preparation and histology preparation.

REFERENCES

1. Tearney GJ, Regar E, Akasaka T, et al. Consensus standards for acquisition, measurement, and reporting of intravascular optical coherence tomography studies: a report from the International Working Group for Intravascular Optical Coherence Tomography Standardization and Validation. J Am Coll Cardiol 2012;59:1058–72.

2. Farooq V, Gogas BD, Okamura T, et al. Three-dimensional optical frequency domain imaging in conventional percutaneous coronary intervention: the potential for clinical application. Eur Heart J 2013;34:875–85.

3. Wang T, Wieser W, Springeling G, et al. Intravascular optical coherence tomography imaging at 3200 frames per second. Opt Lett 2013;38:1715–7.

4. Wieser W, Biedermann BR, Klein T, Eigenwillig CM, Huber R. Multi-megahertz OCT: high quality 3D imaging at 20 million A-scans and 4.5 GVoxels per second. Opt Express 2010;18:14685–704.

ECG-Triggered, Single Cardiac Cycle, High-Speed, 3D, Intracoronary OCT

Recent advances in high-speed intracoronary optical coherence tomography (OCT) have enabled visualization of 3-dimensional (3D) microstructure of long coronary artery segments in vivo (1); however, imaging speed remains insufficient to avoid detrimental cardiac motion artifacts in imaging that spans several cardiac cycles during a pullback, limiting the clinical utility of OCT (2). In addition, the large amount of radiocontrast media used for blood flushing conveys a risk of acute kidney injury. In this study, we report the early experience of high-speed OCT for cardiac motion-free intracoronary imaging in a beating swine heart.

The laboratory-built, high-speed intracoronary OCT comprises an imaging system with an A-line rate of 243 kHz (3), a fiber-optic rotary coupler that sustains rotational speeds up to ~500 revolution/s, and an imaging catheter with a rigid distal length of 3 mm and an outer diameter of 0.87 mm. To avoid bulk cardiac motion during imaging, we implemented prospective triggering using the electrocardiography (ECG) signal. For the starting point of data acquisition and pullback, we gave a relative phase delay (60% of R-R interval) after the final R-wave, which enabled skipping of the QRS complex and T-wave. Accordingly, images recorded during 30% to 40% of the cardiac cycle (a single late diastolic phase) were presumed to be cardiac motion free. For intracoronary imaging in vivo, a male Yorkshire pig (weight 30 kg) was anesthetized and mechanically ventilated. A drug-eluting stent (2.5 × 14 mm) was implanted within the left anterior descending artery. ECG-triggered high-speed imaging (500 frames/s, 100 mm/s) was performed repeatedly ($n = 5$). To mimic conventional OCT operation, low-speed imaging (100 frames/s, 20 mm/s) was also performed ($n = 3$). For clearance of intracoronary blood, iodinated contrast was automatically injected at 3 ml/s during imaging.

In the longitudinal section of ECG-triggered high-speed imaging, the coronary vessel contour appeared smooth and free of discontinuities through the entire pullback length (**Figure 1A**). However, in conventional-speed imaging (**Figure 1B**), the vascular contour was severely distorted at locations that corresponded to systolic and diastolic motion. The cross-sectional OCT images obtained using the high-speed protocol showed comparable resolution, contrast, and depth of penetration compared with conventional-speed imaging. Cutaway longitudinal and fly-through views of the 3D volume rendering revealed the advantage of high-speed OCT more clearly. The 3D architecture of the coronary artery, stent, and guidewire were smoother and more realistic in the ECG-triggered high-speed imaging (**Figure 1C**), whereas the 3D vessel contour appeared inaccurate in conventional imaging (**Figure 1D**). The stent and guidewire looked severely distorted by cardiac motion. Furthermore, the amount of contrast dye delivered by automatic injector during pullback was much smaller in high-speed imaging than in conventional imaging (14 ± 1 ml vs. 21 ± 2 ml, $p = 0.01$).

The combination of the high-speed OCT system, high-speed rotary coupler, optimized high-speed imaging catheter, and prospective ECG triggering has facilitated coronary artery imaging at a rate of 500 frames/s and a pullback speed of 100 mm/s, enabling imaging of a long coronary artery segment during the period of minimal motion artifact within a single cardiac cycle (70 mm pullback in 0.7 s). In addition, the short imaging time decreased the amount of contrast dye required for blood clearing, which would reduce the risk of contrast-induced nephropathy.

Our study has several limitations. First, this was a proof-of-principle study with a limited number of experiments. Second, the system was not tested for

JACC: CARDIOVASCULAR IMAGING, VOL. 9, NO. 5, 2016
MAY 2016:622–36

FIGURE 1 ECG-Triggered High-Speed OCT vs. Conventional-Speed OCT

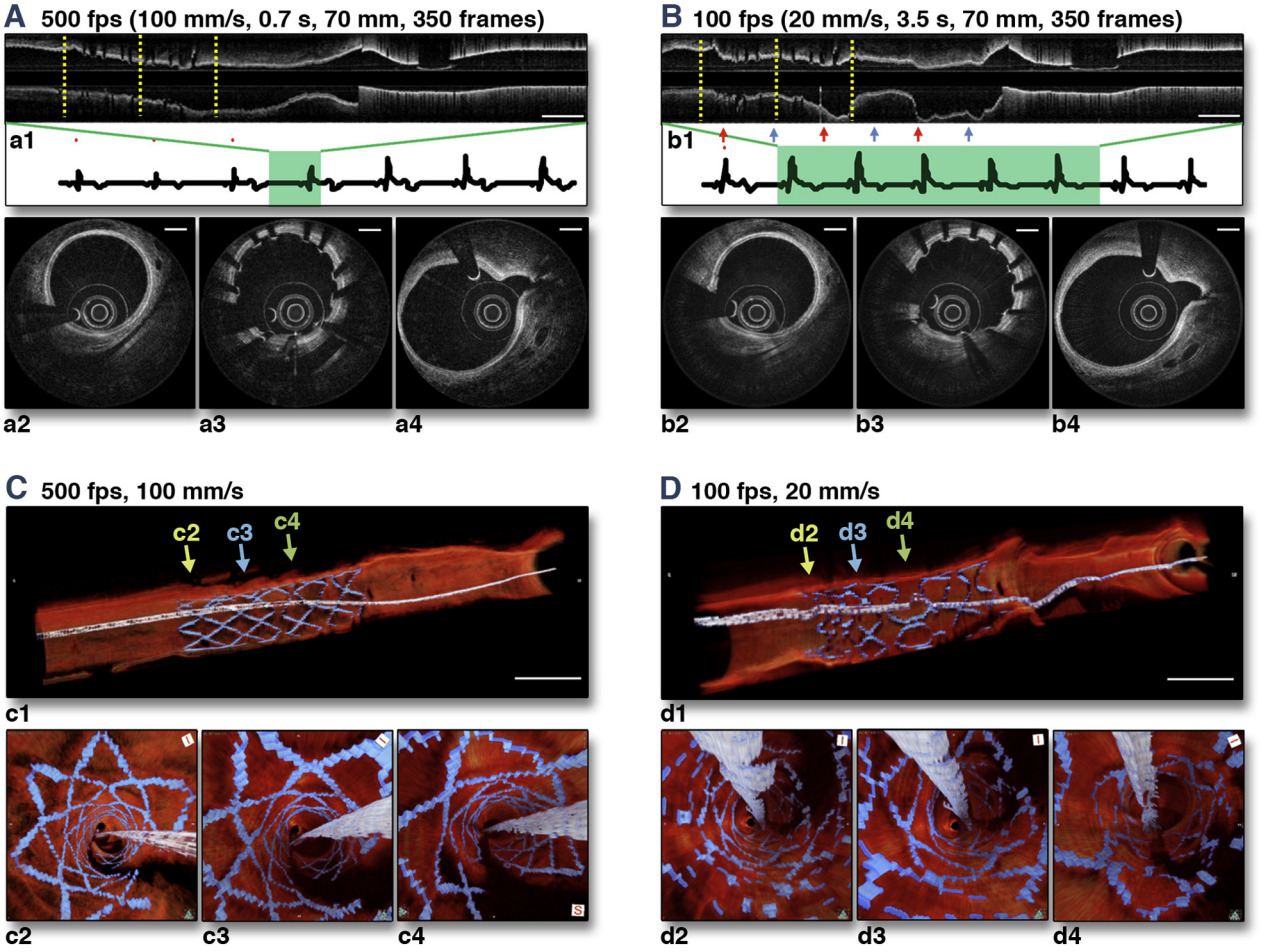

(A) Electrocardiography (ECG)-triggered high-speed optical coherence tomography (OCT). Longitudinal section **(A1)** shows smooth vascular contour. **(B)** Conventional-speed OCT. Longitudinal section **(B1)** shows severe cardiac motion artifacts induced from multiple systolic **(red arrows)** and diastolic **(blue arrows)** motions during a pullback. Cross-sectional images acquired with the ECG-triggered high-speed protocol **(A2-A4** at **yellow dashed lines)** showed comparable quality compared with conventional-speed imaging **(B2-B4). (C)** Three-dimensional (3D) reconstructed images of ECG-triggered high-speed OCT. Both longitudinal and fly-through views show smooth and realistic 3D architecture of the coronary artery, stent, and guidewire. **(D)** 3D reconstructed images of conventional-speed OCT. The cutaway longitudinal view **(D1)** shows distorted 3D vessel contour, stent structure, and guidewire. The fly-through views show disconnected **(D2)** and elongated **(D4)** 3D stent structure, respectively. Scale bars, 5 mm **(A1, B1, C1, D1)** and 500 μm **(A2-A4, B2-B4)**. fps = frames per second.

elevated heart rates, which might have shorter motion-free time windows. Third, the image acquisition was not automatically synchronized with blood flushing. The synchronization of blood flushing and image acquisition along with ECG triggering would further decrease the volume of contrast dye required.

Sun-Joo Jang, MD
Hyun-Sang Park, MS
Joon Woo Song, BS
Tae Shik Kim, MS
Han Saem Cho, MS
Sunwon Kim, MD
Brett E. Bouma, PhD
Jin Won Kim, MD, PhD†
Wang-Yuhl Oh, PhD*

*Department of Mechanical Engineering
Korea Advanced Institute of Science and Technology
291 Daehak-ro, Yuseong-gu
Daejeon 305-701, Republic of Korea
E-Mail: woh1@kaist.ac.kr
OR

†Cardiovascular Center
Korea University Guro Hospital

80 Guro-dong, Guro-gu
Seoul 152-703, Republic of Korea
E-Mail: kjwmm@korea.ac.kr

http://dx.doi.org/10.1016/j.jcmg.2015.11.021

Please note: This study was supported by the National Research Foundation of Korea (grant 2010-0017465, grant 2012R1A2A2A04046108, and Global PhD Fellowship Program [2012H1A2A1010075]), the Ministry of Science, ICT and Future Planning of Korea (grant NIPA-2013-H0401-13-1007), and the National Institutes of Health (grant P41 EB015903). The first 3 authors (Dr. S.-J. Jang, H.-S. Park, and J.W. Song) contributed equally to this work. Drs. W.-Y. Oh and J.W. Kim are joint senior authors.

REFERENCES

1. Tearney GJ, Waxman S, Shishkov M, et al. Three-dimensional coronary artery microscopy by intracoronary optical frequency domain imaging. J Am Coll Cardiol Img 2008;1:752–61.

2. Farooq V, Gogas BD, Okamura T, et al. Three-dimensional optical frequency domain imaging in conventional percutaneous coronary intervention: the potential for clinical application. Eur Heart J 2013;34:875–85.

3. Cho HS, Jang S-J, Kim K, et al. High frame-rate intravascular optical frequency-domain imaging in vivo. Biomed Opt Express 2014;5:223–32.

Noninvasive Quantitative Tissue Characterization of Carotid Plaques Using Color-Coded Mapping Based on Ultrasound Integrated Backscatter

Ultrasound imaging of carotid artery plaques not only identifies the existence and size of the plaques but also provides information on the histological features of the plaques such as lipid pools and fibrous or calcified tissue. We attempted to develop a novel system to obtain the characteristics of carotid plaques using noninvasive ultrasound and high-resolution color-coded display maps based on integrated backscatter (IB) values (the "iPlaque" system).

We prospectively enrolled 17 patients for this study. Seven patients (n = 7 men, 71 ± 5 years old) who underwent carotid artery endarterectomy (CEA) from September 14, 2010 to October 25, 2011 were the group in which we determined the IB thresholds. For validation of the imaging software in our iPlaque system, data were obtained from the following 10 patients (mean age 70 ± 7 years, n = 7 men) who underwent CEA from July 6, 2012 to May 17, 2013. This study was approved by the institutional review board of the University of Tokushima, and each patient gave written informed consent.

Offline imaging analytical software was designed to extract IB values from each pixel of the ultrasound images, which were obtained with commercially available ultrasound diagnostic equipment (Logiq 7, General Electric Medical Systems, Milwaukee, Wisconsin). Cross-sectional scanning of the carotid lesion was performed before surgery, and >20 images/cm that included the largest plaque was stored digitally as RAW data.

In a cross-section of the resected plaques from 7 patients who underwent CEA, we identified 10 sites in each plaque where the histology showed calcification, dense fibrosis, fibrosis, or lipid. Calcification was identified as purple cellular crystals by hematoxylin and eosin staining and brown crystals by Von Kossa staining. Dense fibrosis was identified as intense green staining by Masson trichrome stain or thick orange staining by microscopic polarization after picrosirius red staining. The fibrous portion of the plaque was stained less intensely green by Masson trichrome. The lipid content was visualized as cholesterol clefts on hematoxylin and eosin, Masson trichrome, and oil red O staining.

The IB values of the corresponding locations in the same cross-sectional ultrasound image were calculated. The histological specimen that corresponded to the ultrasonic image was carefully selected by matching the diameter of the vessel and the thickness and shape of the plaque. The IB value was calculated as (tissue value − 255)/255 × dynamic range. The dynamic range was fixed as 40 dB throughout this study. To compensate for the effect of ultrasound attenuation, the IB data in the image were adjusted by 2.0 dB/mm. Each IB value was normalized to the calibrated value by setting the IB value of blood near the plaque at −70 dB. The plaque in the image was manually traced, and then the program calculated the plaque area, area of each tissue component categorized by the IB threshold, and the amount of each component as a percent of the entire plaque area.

The average normalized IB value in 70 sampling points from 7 patients was −37.99 ± 4.93 dB (range −30.14 to −46.00 dB) in dense fibrosis tissue, −52.34 ± 3.99 dB (range −44.73 to −61.23 dB) in fibrosis tissue, and −69.55 ± 5.16 dB (range −60.08 to −79.33 dB) in lipid pool. With a cutoff value of −46.18 dB, dense fibrosis and fibrosis could be discriminated with 97.1% sensitivity and 100% specificity. With a cutoff value of −61.23 dB, fibrosis and lipid pool could be identified with 97.1% sensitivity and 100% specificity. Because the maximum IB value of dense fibrosis was −30.14 dB, a tissue with IB > −30.14 dB was considered to be calcification. Thus, we assigned the following IB thresholds for tissue characterization: calcification −30.14 dB ≤ IB; dense fibrosis −46.18 dB ≤ IB < −30.14 dB; fibrosis −61.23 dB ≤ IB < −46.18 dB; and lipid pool IB < −61.23 dB. With our iPlaque software, calcification is displayed in red, dense fibrosis in yellow, fibrosis in green, and lipid pool in blue. **Figure 1** shows the color-coded